Global and Local Mobility of Apocalmodulin Monitored through Fast-Field Cycling Relaxometry

Valentina Borsi,[†] Claudio Luchinat,[†‡*] and Giacomo Parigi[†‡]
[†]Magnetic Resonance Center (CERM) and [‡]Department of Agricultural Biotechnology, University of Florence, Florence, Italy

ABSTRACT Calmodulin (CaM) is a ubiquitous eukaryotic protein with two conformationally independent domains that can bind up to two calcium ions each. In the calcium-bound state, CaM is able to regulate a vast number of cellular activities by binding to a multiplicity of target proteins in different modes. Its versatility has been ascribed to its anomalously high flexibility. The calcium-free form (apoCaM), which is the resting state of CaM in cells, is also able to functionally bind a number of protein targets, but its dynamics has received less attention. At variance with the calcium-bound form, the crystal structure of apoCaM shows a compact organization of the two domains, but NMR measurements could not detect any contact between them, thus indicating the presence of mobility in solution. The mobility of apoCaM is here investigated through protein proton relaxation rate measurements performed with a high-sensitivity fast-field cycling relaxometer. Such measurements provide direct access to the spectral density function and show that 1), the reorientation time is in agreement with a closed form of the protein; but 2), the collective order parameter is much smaller than for other well folded compact proteins, indicating that a remarkably large side-chain mobility must be present.

INTRODUCTION

Protein dynamics is well established to be fundamental for protein function (1–4), and NMR is a powerful tool for the experimental characterization of protein mobility (5–12). Nuclear spin relaxation measurements (T_1, T_2, and NOE) provide information on motions on the picosecond–nanosecond and microsecond–millisecond timescales (13–15), $T_{1\rho}$ and spin-echo measurements on the microsecond–millisecond timescale (16), and residual dipolar couplings on the picosecond–millisecond timescale, thus covering also the microsecond–nanosecond range (5,17). Such measurements are performed on single nuclei of each protein residue, and thus can be used to monitor the presence of motions related to the individual residues. On the other hand, detailed information of the spectral density function may be recovered, but this is not straightforward.

Fast-field cycling (FFC) relaxometry is a low-resolution technique that consists of measuring nuclear longitudinal relaxation rates as a function of the magnetic fields, from 0.01 to tens or hundreds of MHz (18,19). In this way, the spectral density function of the observed nuclei (typically the solvent water protons) can be directly accessed, and for this reason, it is routinely used for, e.g., the study of contrast agents for magnetic resonance imaging (20–28). Recently, it was shown that relaxometry can be used to detect the collective relaxation rate of protein protons, thus obtaining direct information on their spectral density function (29–32). On the other hand, the intrinsically low sensitivity of this technique provides a unique unresolved signal, so that no information can be obtained on the single protein residues. However, these measurements can be used to define a collective order parameter, S^2_C, which reflects the presence of motions in a range of timescales from picoseconds to nanoseconds (29,31). S^2_C is defined from the reduction in the collective relaxation rate of all nonexchangeable protein protons with respect to the value expected for a rigid protein. Therefore, S^2_C depends on the motional averaging of all kinds of proton-proton interactions, including long-range interactions, which are certainly more sensitive to internal motions. Even short-range interactions may be heavily influenced by local motions, especially for side-chain residues or residues on the protein surface. The measurement of S^2_C can thus provide a further piece of information for the description of the dynamics of proteins.

Particularly interesting cases are those in which proteins, such as multidomain proteins, have domains that experience flexibility. Among these, calmodulin (CaM) is one of the most investigated examples (15,33–38). CaM is a protein of 148 residues highly conserved (>90%) in all eukaryotic cells, and is responsible for regulation of >100 target proteins. It is composed of two domains connected by a central linker. Each of the two domains is constituted by two calcium(II)-binding, highly conserved helix-loop-helix motifs, called EF-hands, with a short, two-stranded antiparallel β-sheet connecting the two loops (39–43).

The structures of both calcium-bound and apoCaM have been solved both in the solid state (44,45) and in solution (33,34,46). Different from the structure of calcium-bound CaM, which in the solid state has an extended conformation, the x-ray structure of apoCaM indicates that the N- and C-terminal domains are close to one another and have a direct interaction (44), leading to a globular shape. On the other hand, solution NMR studies on both forms indicate high flexibility in the central linker region and the absence of

Submitted May 12, 2009, and accepted for publication July 8, 2009.

*Correspondence: luchinat@cerm.unifi.it

Editor: Josh Wand.

0006-3495/09/09/1765/7 $2.00

doi: 10.1016/j.bpj.2009.07.005

stable, direct contacts between the two domains, which are thus free to reorient and experience multiple relative conformations (34,46).

Several NMR techniques have been used to characterize in detail the mobility of calcium-bound CaM (13,15,37,38, 47–49), whereas fewer experiments have been performed to characterize the dynamics of apoCaM. Backbone amide hydrogen exchange experiments suggest that helices in apoCaM are quite mobile (46), and the substantial line broadening observed for a number of residues, especially in the C-terminal domain, indicates that these residues experience a conformational exchange. This supports the idea that flexibility is fundamental for the capability of the C-terminal domain of apoCaM to interact with its target peptides. Furthermore, the calcium-binding loops are found to be particularly unstructured in the calcium-free state, most likely due to their high flexibility (34,46).

Mobility of both apoCaM and calcium-bound CaM in solution has been studied by measuring the amide relaxation rates, a technique providing information on the mobility of the protein backbone. In this way, it was found that the order parameter for all secondary-structure elements is of the order expected for well folded proteins ($S^2 \sim 0.85$ for apoCaM and 0.72 for Ca_4-CaM) when an isotropic diffusion model is used, or when measurements are performed on truncated single-terminal domains of the protein (13–15,50,51). S^2 values down to ~0.55 are obtained for both forms when a global internal motion model is applied to fit the data (13,14). However, whereas the relative mobility of the protein domains of calcium-bound CaM has been extensively studied (37,38), it is not clear how important such mobility is in the apo state of the protein, as the latter has a compact closed structure in the solid state, which also may be the most representative conformation in solution. Furthermore, whereas in calcium-bound CaM side chains have been shown to be exceptionally mobile (49), no information is available on the mobility of side chains of apoCaM. These open questions for apoCaM are addressed here using high-sensitivity FFC relaxometry.

MATERIALS AND METHODS

ApoCaM was expressed and purified as previously reported (52). The apoCaM sample was prepared by dissolving lyophilized apoCaM in D_2O; protein concentration was ~0.6 mM and the pH* was adjusted to 7. Magnetization decay/recovery curves for CaM samples have been obtained at 298 K from 0.02 to 30 MHz using a Stelar FFC relaxometer of the last generation (18). This technique consists of 1), a preparatory part, during which a magnetization is induced through a polarization field (for low-frequency measurements) or a null magnetization is created (for high-frequency measurements), 2), a relaxation part, during which the sample is kept at the relaxation field for a series of time intervals, and 3), a detection part, during which a field of 13 MHz is applied and the magnetization arising after such time intervals is measured. The acquisition is performed by applying a 90° radiofrequency pulse and integrating the resulting proton free-induction decay. The sensitivity of the instrument has been recently improved so that the signal of protein protons in submillimolar protein solutions in D_2O can be detected with a good signal/noise ratio (31). Magnetization decays from a prepolarized intensity were measured for relaxation fields between 0.02 and 10 MHz, using a polarization time of 0.2 s and a polarization field of 30 MHz. The points in the decay were acquired at 48 time values logarithmically scaled between 0.001 and 0.1 s. For the higher fields (10–30 MHz), magnetization recoveries were measured through acquisition of the magnetization signal for 64 time values logarithmically scaled between 0.002 and 0.8 s. The numbers of scans were 512 and 128 for the decay and recovery curves, respectively.

The "universal" distribution of the relaxation rates reported in Luchinat and Parigi (31) was used to fit the magnetization decay/recovery. The fit function for the magnetization decay curves (up to 10 MHz) was $M = P1 + P2 \times (0.0076 \times \exp(-P3 \times t \times 0.11) + 0.0079 \times \exp(-P3 \times t \times 0.13) + 0.0051 \times \exp(-P3 \times t \times 0.16) + 0.0098 \times \exp(-P3 \times t \times 0.19) + 0.0166 \times \exp(-P3 \times t \times 0.229) + 0.0234 \times \exp(-P3 \times t \times 0.275) + 0.0267 \times \exp(-P3 \times t \times 0.331) + 0.0316 \times \exp(-P3 \times t \times 0.398) + 0.0532 \times \exp(-P3 \times t \times 0.479) + 0.0673 \times \exp(-P3 \times t \times 0.575) + 0.0784 \times \exp(-P3 \times t \times 0.692) + 0.102 \times \exp(-P3 \times t \times 0.832) + 0.1223 \times \exp(-P3 \times t \times 1.) + 0.0881 \times \exp(-P3 \times t \times 1.202) + 0.0566 \times \exp(-P3 \times t \times 1.445) + 0.0588 \times \exp(-P3 \times t \times 1.74) + 0.0751 \times \exp(-P3 \times t \times 2.09) + 0.0849 \times \exp(-P3 \times t \times 2.512) + 0.0575 \times \exp(-P3 \times t \times 3.02) + 0.0208 \times \exp(-P3 \times t \times 3.63) + 0.0069 \times \exp(-P3 \times t \times 4.37))$, where M is the magnetization, t is the time, and $P1$, $P2$, and $P3$ are fit parameters. The relaxation rates present in the distribution are thus provided by $P3$ times the different numbers in the exponential functions. For the magnetization recovery curves (for frequencies >10 MHz), the same function is used with exp() substituted to $1 - \exp()$ and an additional term $(1 - \exp(-0.06 \times t)$ added to include the relaxation recovery of free water protons in D_2O.

RESULTS

The collective protein proton relaxation rate was calculated for each field of measurement from the fit of the magnetization decay/recovery curve using the "universal" relaxation rate distribution obtained for well folded proteins (31), reported in Material and Methods, and the fits were quite satisfactory (Fig. 1), with reduced χ^2 sizably smaller (by a factor of 4–1.5) than that obtained with monoexponential fits. Such collective relaxation rate values, corresponding to the weighted average of the relaxation rates of all nonexchangeable protons in the protein, are reported as a function of field in Fig. 2. No difference in the relaxation profile was observed when the concentration of the protein was decreased to 0.3 or increased to 1.2 mM. This indicates that there is no protein aggregation, because the latter would be reflected in increasing contributions from molecules with a larger reorientation time. The relaxation profile shows one dispersion around 10 MHz; in general, such dispersion is related to a correlation time in the spectral density function that corresponds to the reorientation time of the protein (29,31). The profile was fit to Eq. 1:

$$R_1 = S_C^2 \langle E^2 \rangle \left(\frac{0.8\tau_R}{1 + 4\omega^2\tau_R^2} + \frac{0.2\tau_R}{1 + \omega^2\tau_R^2} \right) + \alpha, \qquad (1)$$

where τ_R, S_C^2, and α are fit parameters. The validity of this equation for the collective protein proton relaxation rates as a function of the field was demonstrated by simulations performed using relaxation data generated with CORMA

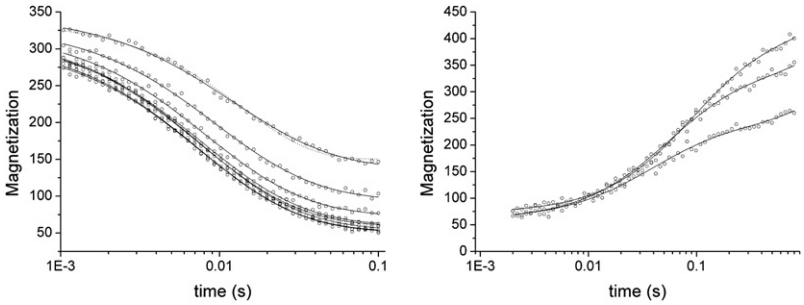

FIGURE 1 (*Left*) Magnetization decays at low magnetic fields (2.8, 1.5, 0.8, 0.4, 0.2, 0.1, 0.07, and 0.04 MHz, from top to bottom). The monoexponential fit is shown as a dotted line for the magnetization decay at 2.8 MHz. (*Right*) Magnetization recovers at high magnetic fields (30, 20, and 14 MHz, from top to bottom). In both panels, best-fit lines were calculated using the ''universal'' distribution of the relaxation rates defined in Luchinat and Parigi (31) and described in the Materials and Methods section of this work.

(31). However, the same equation (as well as the equation commonly used for unlike spins, due to the onset of the cross relaxation/spin diffusion effects at high fields) would be incorrect for the individual proton relaxation dispersions (31).

From the average of all proton-proton dipolar interactions using the program CORMA (53,54) and the structure of apoCaM (PDB 1QX5), $\langle E^2 \rangle$ was calculated to be 26.0×10^9 s^{-2} (25.4×10^9 s^{-2} if the 1LKJ_1 structure is used). $\langle E^2 \rangle$ can also be obtained from the measurement of the second moment as achievable from the free-induction decay of the NMR signal of the protein in the solid state. For largely hydrated proteins, the second moment nicely matches with the $S_C^2 \langle E^2 \rangle$ value obtained from low-field relaxation measurements (30,31). (The second moment of a dry protein can be different from that of the hydrated system due to protein structural changes occurring in the presence of water (30). It has also been shown that hydration decreases the measured second moment because the latter is affected by the motional freedom experienced by the side chains, so that when the high-hydration plateau is reached, it becomes a measure of $S_C^2 \langle E^2 \rangle$ rather than of $\langle E^2 \rangle$.) The $\langle E^2 \rangle$ value, although dependent on the local accuracy of the protein structural model, because it is a function of the sixth power of the distance between close protons, has been shown to be relatively constant and equal to $(27 \pm 3) \times 10^9$ s^{-2} in a large variety of regularly folded proteins (31). This is due to the fact that the major contribution to $\langle E^2 \rangle$ is given by the dipolar interactions between protons belonging to the same methylene and methyl groups, which have a fixed distance. The accuracy of the estimate of $\langle E^2 \rangle$ reflects on the accuracy of the determined S_C^2 value.

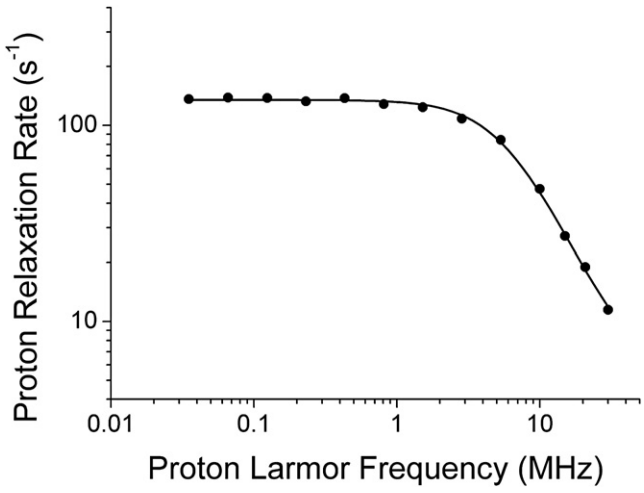

FIGURE 2 Collective protein proton relaxation rates for 0.6 mM apocalmodulin, calculated as the weighted average of the relaxation rates obtained from the ''universal'' distribution (31). The solid line shows the best-fit profile according to Eq. 1.

The best-fit value of τ_R is 13.6 $\pm$ 0.5 ns, and it represents the correlation time modulating the dipolar interactions, i.e., the reorientation time of the protein (the error is estimated from the standard deviation). This value is in good agreement with the harmonic mean correlation time calculated by HYDRONMR (55) from the anisotropic rotational diffusion tensor using the x-ray structure of apoCaM (PDB 1QX5) in D_2O at 298 K, equal to 14.0 ns. The harmonic mean reorientation time calculated by HYDRONMR using the apoCaM extended solution structure (1LKJ_1) is 19 ns, and it decreases to 15 ns for other structures reported within the same family, where the two domains are differently oriented and closer to one another; the harmonic mean reorientation times of individual N-terminal (residues 1–80) and C-terminal (residues 81–146) domains are 7.9 and 5.5 ns, respectively. Therefore, the experimentally obtained τ_R value indicates that also in solution the reorientation time of apoCaM is basically the same as that of the protein with the two domains in a closed position; this indicates that the protein would preferentially assume one or more compact structures. This is in line with other biochemical and biophysical measurements (56) (see below), and not in contrast to the NMR solution studies. Indeed, the latter indicate a lack of structural interaction between the two protein domains and mobility of the interdomain linker, both of which phenomena are still consistent with a fluxional behavior of the domains resulting in an ensemble of ''closed'' conformations.

The best-fit value for the squared collective order parameter, S_C^2, related to the global protein reorientation time, is 0.37 $\pm$ 0.02 (mean $\pm$ SD). The accuracy of this parameter can be estimated to be ~0.07 as a consequence of the accuracy of the calculated $\langle E^2 \rangle$ value, in the hypothesis of a single correlation time responsible for the observed dispersion. This value is, beyond any experimental uncertainty, much smaller than that found for lysozyme and albumin (29), where S_C^2

TABLE 1 Summary of best-fit correlation times and order parameters obtained for apoCaM

	Isotropic model		Global internal motion model			
	τ_R (ns)	S^2_C	τ_{R1} (ns)	$S^2_{C(1)}$	τ_{R2} (ns)	$S^2_{C(2)}$
Low-field relaxation (this work)	13.6	0.37	14.4	0.32	6.5 (fixed)	0.06
			14.0	0.35	3.7 (fixed)	0.05
High-field relaxation(14)	9.1–10.3*	0.85	11.8–16.7*	0.53–0.60	2.7–4.2*	0.25–0.32

*Values are scaled by the factor 1.11/0.9 = 1.23 for comparison with the values in D_2O used in this study.

was calculated to be ~0.75. This indicates that internal dynamics in apoCaM must be much more effective than in the latter proteins.

The parameter α represents the protein proton collective relaxation value achieved when the τ_R dispersion is completed. Therefore, it is given by the contribution to relaxation of the $(1 - S^2_C)$ term times the spectral density function related to local motions and occurring at timescales faster than those observable in the detected field range. From the value of α as obtained from the fit of the experimental profile to Eq. 1 ($\alpha = 4.2 \pm 0.6\ s^{-1}$), correlation time values of ~0.2 ns are obtained for the fast local motions, using the relationship $\alpha = (1 - S^2_C)\langle E^2\rangle\langle\tau_{fast}\rangle$. We note that in this case, the value of α is about double the value obtained for lysozyme and albumin (29,31), consistent with the much larger $(1 - S^2_C)$ value.

^{15}N relaxation studies indicated that the two CaM domains experience a restricted mobility superimposed on the overall tumbling of the molecule (14). Further analyses were thus performed to investigate whether the reduction in S^2_C with respect to the values obtained for the other proteins can be ascribed to the motion of the single domains (global internal motion model). Therefore, the relaxation profile of apoCaM was fit using two collective order parameters and two correlation times, with one of these times fixed at 6.5 ns, i.e., around that of the individual domains of the protein, to possibly detect the effect of an independent restricted reorientational motion of the two domains, according to Eq. 2.

$$R_1 = \langle E^2\rangle\left[S^2_{C(1)}\left(\frac{0.8\tau_{R1}}{1 + 4\omega^2\tau^2_{R1}} + \frac{0.2\tau_{R1}}{1 + \omega^2\tau^2_{R1}}\right) + S^2_{C(2)}\left(\frac{0.8\tau_{R2}}{1 + 4\omega^2\tau^2_{R2}} + \frac{0.2\tau_{R2}}{1 + \omega^2\tau^2_{R2}}\right)\right] + \alpha. \quad (2)$$

The fit was equally good, and a first reorientation time of 14.4 ns is calculated with $S^2_{C(1)} = 0.32$; the $S^2_{C(2)}$ corresponding to the motion at 6.5 ns was calculated to be 0.06, i.e., much smaller (see Table 1). The presence of multiple correlation times cannot thus increase the S^2_C value corresponding to the slowest motion. This proves that the reduction in the S^2_C value observed for CaM with respect to the other proteins is indeed almost independent of the number of correlation times used to fit the data, and that the value itself is quite robust. It also proves that the fastest motions occur predominantly on timescales shorter than that expected for the reorientation of the single domains.

DISCUSSION

The calculated reorientation time indicates that for most of the time the protein maintains a relatively compact structure, and thus that the two domains must be close to one another even in solution, although the absence of interdomain NOEs (34) suggests that a dynamic ensemble of conformations must be experienced. This is a relevant finding and is in line with the observation of interdomain contacts in apoCaM in solution through fluorescence spectroscopy measurements performed on engineered apoCaM mutants (57). Fluorescence resonance energy transfer measurements (58) also suggest a reorientation time in agreement with the overall protein rotational motion, indicating that the interdomain conformational heterogeneity detected through high-field NMR measurements must be the result of a number of slowly interconverting (on the nanosecond timescale) distinct conformations (58).

^{15}N relaxation studies previously performed (14) indicate a shorter reorientation time when an isotropic model for protein tumbling is assumed, shorter than expected for a fully compact closed structure. This made the global internal motion model, where internal domains have a restricted mobility superimposed on the overall tumbling of the molecule, preferable, as did the significantly better agreement between experimental and best-fit values achieved with this model. The global reorientation times obtained from the high-field relaxation measurements are largely affected by the selected groups of residues included in the fit and by the fields of measurement, and their uncertainty is thus relatively large. In the case of apoCaM, the reorientation times range from 9.6 to 13.6 ns in H_2O (14). Scaled to D_2O, they range from 11.8 to 16.7 ns, which compares well with the best-fit τ_R value of 14 ns in this study (Table 1).

The fit of the high-field relaxation data also indicates the occurrence of internal motions with a correlation time of ~3 ns (14). The latter time seems to be too short for the tumbling of the CaM single domains, which is expected to take ~5–5.5 ns in H_2O. The fit of the data described here actually indicates that if a motion with a correlation time in this range is present, its order parameter must be quite low (see Table 1). On the other hand, a fit of equally good quality was also obtained by fixing the internal correlation time to 3.7 ns (corresponding to 3 ns in H_2O), as found in the ^{15}N relaxation study, the other parameters assuming values between those calculated in the isotropic model and those

in the internal motion model with τ_{R2} fixed to 6.5 ns (see Table 1). In conclusion, the data presented here are not sensitive enough to determine the presence of motions with correlation times of the order of some nanoseconds, and they are consistent with the presence of such motions only with collective squared order parameters <0.1. For the purpose of this study, it is important to note that the presence of such internal motions does not sizably change the value of the overall tumbling or of the corresponding order parameter.

As expected, the obtained S^2_C values are smaller than the available S^2 values obtained from relaxation rate measurements on backbone nuclei at high fields (50), in the assumption of both an isotropic model with a single reorientation time ($S^2 = 0.85$) or a global internal motion model, described by two order parameters, one for the global reorientation and one for internal protein motions occurring on an intermediate timescale between the global reorientation time and the faster internal dynamics. In the latter model, in fact, an averaged $S^2_{NH(1)}$ value of 0.56 was calculated from the amide relaxation with a correlation time corresponding to the overall reorientation time of the protein (14), and further $S^2_{NH(2)}$ values of 0.25–0.30 for a correlation time of 2.5–3 ns (see Table 1). Both of these values are significantly larger (outside the error) than the $S^2_{C(1,2)}$ values of 0.32 and 0.06 obtained from the fit of the data presented here.

Comparison of the order parameters determined from high-field data and the collective S^2_C values determined here actually shows that the former does not monitor all motional features present in the protein in the picosecond–nanosecond range. This is because side-chain dynamics is not revealed. On the other hand, side-chain dynamics may be fundamental in the characterization of the protein. For instance, the low sensitivity of ^{15}N relaxation measurements to side-chain and protein-domain motions is indicated by the fact that the S^2_{NH} values obtained for the calcium-bound CaM in the absence and presence of bound peptides are essentially the same for all residues except those in the linker between the N-terminal and C-terminal domains, despite the fact that the difference in the dynamics within the protein is outstanding (15,47). Analogously, only slightly different squared order parameters were calculated for the ^{13}CO-^{13}Cα vectors for free and complexed CaM (15).

Side-chain mobility is better addressed by the model-free generalized order parameter, S^2_{axis} for the symmetry axis of methyl groups (59). From the methyl order parameters observed in calcium-bound CaM, three distinct classes of motions were suggested, centered at squared order parameters of 0.35, 0.58, and 0.78, and for some methyl groups, peptide binding was shown to increase substantially the S^2_{axis} measured, by often moving methyls from one lower order-parameter group to a larger order-parameter group (48,59). These works clearly show that CaM has a peculiar enhanced mobility in the side chains. As suggested by Lee et al. (49), this may be due to the hydrophobic residues allowing much larger side-chain mobility than in the side chains of canonical globular proteins. In our study, the collective S^2_C value found for apoCaM (0.37), dramatically smaller than the value observed for other well folded globular proteins (0.75) (29,31), is even on the lowest side of the range of the S^2_{axis} values for methyl groups (59). In this context, it is particularly significant that the S^2_C values obtained using this approach arise from all protein protons, three-fourths of which belong to side chains, rather than from methyl protons, which constitute approximately one-fourth of the total. The strikingly small S^2_C value obtained in this work points to an extraordinary mobility not only of methyl groups but of side-chain protons in general.

Such high mobility of side-chain protons is not shared by backbone protons, as it results from ^{15}N relaxation data. This makes it possible that the ''universal'' distribution of relaxation rates that was used to fit the data, and which indeed provided a good fit of the magnetization decay/recovery curves, may not approximate the real distribution as satisfactorily as it does for more rigid globular proteins. A fit of the magnetization decay/recovery curves was thus also performed using a double-exponential function instead of the ''universal'' rate distribution, and in this case also the agreement with the experimental data was very good, the resulting relaxation rates being about 10% smaller. Therefore, the fit of the resulting profile provides basically the same best-fit parameters, with an S^2_C value only slightly smaller.

Relaxation measurements performed on apoCaM showed that the chemical exchange contributions are substantial for most residues of the C-terminal domain, thus implying intradomain exchange between conformational substates (50). This intradomain conformational exchange appears to involve transitions between a predominantly populated closed conformation (with an antiparallel helical arrangement) and a smaller population of more open conformations (not parallel helical arrangements) of the C-terminal domain (34,46,50,60–64). A dynamic equilibrium involving conformations with a partially exposed hydrophobic core provides CaM with the ability to interact with its targets in the absence of excess calcium(II) (65,66). Therefore, EF-hand motifs in apoCaM exist in both the closed and open states, possibly sampling a very large spectrum of conformational states, with a conformational exchange rate on the microsecond–millisecond timescale and predominance of the closed conformation. Although the generalized order parameter S^2_C obtained here only reflects motions in a range of timescales from the picoseconds to the nanoseconds, the presence of a large mobility in these scales is likely to be associated with mobility in a slower scale as well.

Large mobility also seems to be present in the N-terminal domain, and not only within the residues corresponding to the calcium binding loops. It was in fact shown that the first helix of the N-terminal domain of apoCaM undergoes large-amplitude nanosecond motions (67). This indicates a considerable dynamic flexibility of the first helix of the N-terminal domain, and thus within the domain, in apoCaM. This is in

line with molecular dynamics simulations that predicted the presence within the amino-terminal domain of the protein of four subdomains that have the potential to undergo large-amplitude independent motions relative to one another (36).

In conclusion, the measurements here presented for apoCaM provide direct information on both the reorientation time of the investigated system and the extent of internal motions of protein protons. It is found that 1), the reorientation time obtained from the fit of the spectral density function of protein protons indicates that the protein is mainly in a conformation with the two domains in close contact; and 2), the collective squared order parameter obtained in this analysis is much smaller than that obtained for other globular proteins. Such low S_C^2 value depends on the larger side-chain dynamics of apoCaM, because three-fourths of the protons contributing to the S_C^2 value belong to side chains, and backbone nuclei are known from ^{15}N high-field relaxation measurements to have a regular mobility. Therefore, $S_C{}^2$ beautifully complements other measurements to describe the extent of both global and local motional features experienced by the system.

Protein proton relaxation measurements at low fields, providing direct access to the spectral density function, thus allow us to safely recover the reorientation time of the protein, which at high fields may prove less straightforward to obtain because the corresponding dispersion has occurred already largely. From the reorientation time value, further information can be derived on the conformational state of the investigated systems. Protein proton relaxation measurements at low fields also provide a collective order parameter that monitors side-chain mobility, which is not accounted for in standard high-field ^{15}N relaxation measurements. These findings point out some global aspects of the motion that complement other aspects available using different techniques, so that all the data together can provide a complete picture for the protein dynamics. The approach here proposed can be even more relevant for mobility studies of large proteins, when information from high-field ^{15}N T_1, T_2, and NOE measurements can hardly be obtained due to severe line broadening of the NMR spectra, as well as for the investigation of dynamics in protein-protein adducts.

This work was supported by Ente Cassa di Risparmio di Firenze and by the European Commission (contracts Bio-DNP 011721 and EU-NMR 026145).

REFERENCES

1. Wang, L. C., Y. X. Pang, T. Holder, J. R. Brender, A. V. Kurochkin, et al. 2001. Functional dynamics in the active site of the ribonuclease binase. *Proc. Natl. Acad. Sci. USA.* 98:7684–7689.
2. Eisenmesser, E. Z., D. A. Bosco, M. Akke, and D. Kern. 2002. Enzyme dynamics during catalysis. *Science.* 295:1520–1523.
3. Lindorff-Larsen, K., R. B. Best, M. A. DePristo, C. M. Dobson, and M. Vendruscolo. 2005. Simultaneous determination of protein structure and dynamics. *Nature.* 433:128–132.
4. Fragai, M., C. Luchinat, and G. Parigi. 2006. "Four-dimensional" protein structures: examples from metalloproteins. *Acc. Chem. Res.* 39:909–917.
5. Lange, O. F., N.-A. Lakomek, C. Farès, G. F. Schröder, K. F. A. Walter, et al. 2008. Recognition dynamics up to microseconds revealed from an RDC-derived ubiquitin ensemble in solution. *Science.* 320: 1471–1475.
6. Valentine, E. R., and A. G. Palmer. 2005. Microsecond-to-millisecond conformational dynamics demarcate the GluR2 glutamate receptor bound to agonists glutamate, quisqualate, and AMPA. *Biochemistry.* 44:3410–3417.
7. Ryabov, Y. E., and D. Fushman. 2007. A model of interdomain mobility in a multidomain protein. *J. Am. Chem. Soc.* 129:3315–3327.
8. Ishima, R., and D. A. Torchia. 2000. Protein dynamics from NMR. *Nat. Struct. Biol.* 7:740–743.
9. Mulder, F. A. A., A. Mittermaier, B. Hon, F. W. Dahlquist, and L. E. Kay. 2001. Studying excited states of proteins by NMR spectroscopy. *Nat. Struct. Biol.* 8:932–935.
10. Kay, L. E. 2005. NMR studies of protein structure and dynamics. *J. Magn. Reson.* 173:193–207.
11. Fischer, M. W. F., L. Zeng, A. Majumdar, and E. R. P. Zuiderweg. 1998. Characterizing semilocal motions in proteins by NMR relaxation studies. *Proc. Natl. Acad. Sci. USA.* 95:8016–8019.
12. Brüschweiler, R. 2003. New approaches to the dynamic interpretation and prediction of NMR relaxation data from proteins. *Curr. Opin. Struct. Biol.* 13:175–183.
13. Baber, J. L., A. Szabo, and N. Tjandra. 2001. Analysis of slow interdomain motion of macromolecules using NMR relaxation data. *J. Am. Chem. Soc.* 123:3953–3959.
14. Tjandra, N., H. Kuboniwa, H. Ren, and A. Bax. 1995. Rotational dynamics of calcium-free calmodulin studied by ^{15}N-NMR relaxation measurements. *Eur. J. Biochem.* 230:1014–1024.
15. Wang, T., K. K. Frederick, T. I. Igumenova, A. J. Wand, and E. R. P. Zuiderweg. 2005. Changes in calmodulin main-chain dynamics upon ligand binding revealed by cross-correlated NMR relaxation measurements. *J. Am. Chem. Soc.* 127:828–829.
16. Akke, M., and A. G. Palmer, III. 1996. Monitoring macromolecular motions on microsecond to millisecond time scales by R_{1rho}-R_1 constant relaxation time NMR spectroscopy. *J. Am. Chem. Soc.* 118:911–912.
17. Fushman, D., R. Varadan, M. Assfalg, and O. Walker. 2004. Determining domain orientation in macromolecules by using spin-relaxation and residual dipolar coupling measurements. *Prog. Nucl. Magn. Reson. Spectrosc.* 44:189–214.
18. Ferrante, G., and S. Sykora. 2005. Technical aspects of fast field cycling. *Adv. Inorg. Chem.* 57:405–470.
19. Kimmich, R., and E. Anoardo. 2004. Field-cycling NMR relaxometry. *Prog. Nucl. Magn. Reson. Spectrosc.* 44:257–320.
20. Aime, S., P. L. Anelli, M. Botta, M. Brocchetta, S. Canton, et al. 2002. Relaxometric evaluation of novel manganese(II) complexes for application as contrast agents in magnetic resonance imaging. *J. Biol. Inorg. Chem.* 7:58–67.
21. Kowalewski, J., and L. Maler. 2006. Nuclear Spin Relaxation in Liquids: Theory, Experiments, and Applications. Taylor & Francis, London.
22. Kowalewski, J., D. Kruk, and G. Parigi. 2005. NMR relaxation in solution of paramagnetic complexes: recent theoretical progress for $S > 1$. *Adv. Inorg. Chem.* 57:41–104.
23. Schühle, D. T., J. Schatz, S. Laurent, L. Vander Elst, R. N. Muller, et al. 2009. Calix[4]arenes as molecular platforms for magnetic resonance imaging (MRI) contrast agents. *Chemistry (Easton).* 15:3290–3296.
24. Assfalg, M., E. Gianolio, S. Zanzoni, S. Tomaselli, V. Lo Russo, et al. 2007. NMR structural studies of the supramolecular adducts between a liver cytosolic bile acid binding protein and gadolinium(III)-chelates bearing bile acids residues: molecular determinants of the binding of a hepatospecific magnetic resonance imaging contrast agent. *J. Med. Chem.* 50:5257–5268.
25. Rinck, P. A., H. W. Fischer, L. Vander Elst, Y. Van Haverbeke, and R. N. Muller. 1988. Field-cycling relaxometry: medical applications. *Radiology.* 168:843–849.

26. Major, J. L., T. J. Meade, G. Parigi, and C. Luchinat. 2007. The synthesis and in-vitro testing of a Zn(II)-activated MR contrast agent. *Proc. Natl. Acad. Sci. USA.* 104:13881–13886.
27. Urbanczyk-Pearson, L. M., F. J. Femia, J. Smith, G. Parigi, C. Luchinat, et al. 2008. Mechanistic investigation of β-galactosidase-activated MR contrast agents. *Inorg. Chem.* 47:56–68.
28. Caravan, P., N. Cloutier, S. McDermid, J. J. Ellison, J. M. Chasse, et al. 2007. Albumin binding, relaxivity and water exchange kinetics of the diastereoisomers of MS-325 a gadolinium(III) based magnetic resonance angiography contrast agent. *Inorg. Chem.* 46:6632–6639.
29. Bertini, I., Y. K. Gupta, C. Luchinat, G. Parigi, C. Schlörb, et al. 2005. NMR spectroscopic detection of protein protons and longitudinal relaxation rates between 0.01 and 50 MHz. *Angew. Chem. Int. Ed.* 44:2223–2225.
30. Diakova, G., Y. A. Goddard, J.-P. Korb, and R. G. Bryant. 2007. Changes in protein structure and dynamics as a function of hydration from 1H second moments. *J. Magn. Reson.* 189:166–172.
31. Luchinat, C., and G. Parigi. 2007. Collective relaxation of protein protons at very low magnetic field: a new window on protein dynamics and aggregation. *J. Am. Chem. Soc.* 129:1055–1064.
32. Korb, J.-P., and R. G. Bryant. 2001. The physical basis for the magnetic field dependence of proton spin-lattice relaxation rates in proteins. *J. Chem. Phys.* 115:10964–10974.
33. Barbato, G., M. Ikura, L. E. Kay, R. W. Pastor, and A. Bax. 1992. Backbone dynamics of calmodulin studied by ^{15}N relaxation using inverse detected two-dimensional NMR spectroscopy; the central helix is flexible. *Biochemistry.* 31:5269–5278.
34. Kuboniwa, H., N. Tjandra, S. Grzesiek, H. Ren, C. B. Klee, et al. 1995. Solution structure of calcium-free calmodulin. *Nat. Struct. Biol.* 2: 768–776.
35. Evenäs, J., S. Forsén, A. Malmendal, and M. Akke. 1999. Backbone dynamics and energetics of a calmodulin domain mutant exchanging between closed and open conformations. *J. Mol. Biol.* 289:603–617.
36. Wriggers, W., E. Mehler, F. Pitici, H. Weinstein, and K. Schulten. 1998. Structure and dynamics of calmodulin in solution. *Biophys. J.* 74:1622–1639.
37. Bertini, I., C. Del Bianco, I. Gelis, N. Katsaros, C. Luchinat, et al. 2004. Experimentally exploring the conformational space sampled by domain reorientation in calmodulin. *Proc. Natl. Acad. Sci. USA.* 101:6841–6846.
38. Bertini, I., Y. K. Gupta, C. Luchinat, G. Parigi, M. Peana, et al. 2007. Paramagnetism-based NMR restraints provide maximum allowed probabilities for the different conformations of partially independent protein domains. *J. Am. Chem. Soc.* 129:12786–12794.
39. Chou, J. J., S. Li, C. B. Klee, and A. Bax. 2001. Solution structure of Ca2+ calmodulin reveals flexible hand-like properties of its domains. *Nat. Struct. Biol.* 8:990–997.
40. Yuan, T., H. Ouyang, and H. J. Vogel. 1999. Surface exposure of the methionine side chains of calmodulin in solution. *J. Biol. Chem.* 274:8411–8420.
41. Schumacher, R. T., A. F. Rivard, H. P. Bachinger, and J. P. Adelman. 2001. Structure of the gating domain of a Ca^{2+}-activated K^+ channel complexed with Ca^{2+}/calmodulin. *Nature.* 410:1120–1124.
42. Ikura, M., G. M. Clore, A. M. Gronenborn, G. Zhu, C. Clee, et al. 1992. Solution structure of a calmodulin-target peptide complex by multidimensional NMR. *Science.* 256:632–638.
43. Ikura, M., G. Barbato, C. B. Klee, and A. Bax. 1992. Solution structure of calmodulin and its complex with a myosin light chain kinase fragment. *Cell Calcium.* 13:391–400.
44. Schumacher, M. A., M. Crum, and M. C. Miller. 2004. Crystal structures of apocalmodulin and apocalmodulin/SK potassium channel gating domain complex. *Structure.* 12:849–860.
45. Babu, Y. S., C. E. Bugg, and W. J. Cook. 1988. Structure of calmodulin refined at 2.2 Å resolution. *J. Mol. Biol.* 204:191–204.
46. Zhang, M., T. Tanaka, and M. Ikura. 1995. Calcium-induced conformational transition revealed by the solution structure of apo calmodulin. *Nat. Struct. Biol.* 2:758–767.
47. Igumenova, T. I., A. L. Lee, and A. J. Wand. 2005. Backbone and side chain dynamics of mutant calmodulin-peptide complexes. *Biochemistry.* 44:12627–12639.
48. Frederick, K. K., M. S. Marlow, K. G. Valentine, and A. J. Wand. 2007. Conformational entropy in molecular recognition by proteins. *Nature.* 448:325–329.
49. Lee, A. L., S. A. Kinnear, and A. J. Wand. 2000. Redistribution and loss of side chain entropy upon formation of a calmodulin-peptide complex. *Nat. Struct. Biol.* 7:72–77.
50. Malmendal, A., J. Evenäs, S. Forsén, and M. Akke. 1999. Structural dynamics in the C-terminal domain of calmodulin at low calcium levels. *J. Mol. Biol.* 293:883–899.
51. Urbauer, J. L., J. H. Short, L. K. Dow, and A. J. Wand. 1995. Structural analysis of a novel interaction by calmodulin: high-affinity binding of a peptide in the absence of calcium. *Biochemistry.* 34:8099–8109.
52. Bertini, I., I. Gelis, N. Katsaros, C. Luchinat, and A. Provenzani. 2003. Tuning the affinity for lanthanides of calcium binding proteins. *Biochemistry.* 42:8011–8021.
53. Keepers, J. W., and T. L. James. 1984. A theoretical study of distance determinations from NMR. Two-dimensional nuclear Overhauser effect spectra. *J. Magn. Reson.* 57:404–426.
54. Borgias, B., M. Gochin, D. J. Kerwood, and T. L. James. 1990. Relaxation matrix analysis of 2D NMR data. *Prog. Nucl. Magn. Reson. Spectrosc.* 22:83–100.
55. Garcìa de la Torre, J., M. L. Huertas, and B. Carrasco. 2000. HYDRONMR: prediction of NMR relaxation of globular proteins from atomic-level structures and hydrodynamic calculations. *J. Magn. Reson.* 147:138–146.
56. Qin, Z., and T. C. Squier. 2001. Calcium-dependent stabilization of the central sequence between Met^{76} and Ser^{81} in vertebrate calmodulin. *Biophys. J.* 81:2908–2918.
57. Boschek, C. B., T. C. Squier, and D. J. Bigelow. 2007. Disruption of interdomain interactions via partial calcium occupancy of calmodulin. *Biochemistry.* 46:4580–4588.
58. Sun, H., D. Yin, and T. C. Squier. 1999. Calcium-dependent structural coupling between opposing globular domains of calmodulin involves the central helix. *Biochemistry.* 38:12266–12279.
59. Marlow, M. S., and A. J. Wand. 2006. Conformational dynamics of calmodulin in complex with the calmodulin-dependent kinase kinase α calmodulin-binding domain. *Biochemistry.* 45:8732–8741.
60. Evenas, J., A. Malmendal, E. Thulin, G. Carlström, and S. Forsén. 1998. Ca^{2+} binding and conformational changes in a calmodulin domain. *Biochemistry.* 37:13744–13754.
61. Capozzi, F., C. Luchinat, C. Micheletti, and F. Pontiggia. 2007. Essential dynamics of helices provide a functional classification of EF-hand proteins. *J. Proteome Res.* 6:4245–4255.
62. Babini, E., I. Bertini, F. Capozzi, C. Luchinat, A. Quattrone, et al. 2005. Principal component analysis of a comprehensive structural database of EF-hand domains to describe the conformational freedom within the EF-hand superfamily. *J. Proteome Res.* 4:1961–1971.
63. Houdusse, A., M. Silver, and C. Cohen. 1996. A model of Ca^{2+}-free calmodulin binding to unconventional myosins reveals how calmodulin acts as a regulatory switch. *Structure.* 4:1475–1490.
64. Evenäs, J., A. Malmendal, and M. Akke. 2001. Dynamics of the transition between open and closed conformations in a calmodulin C-terminal domain mutant. *Structure.* 9:185–195.
65. Chin, D. H., and A. R. Means. 2000. Calmodulin: a prototypical calcium sensor. *Trends Cell Biol.* 10:322–328.
66. Houdusse, A., J.-F. Gaucher, E. Krementsova, S. Mui, K. M. Trybus, et al. 2006. Crystal structure of apo-calmodulin bound to the first two IQ motifs of myosin V reveals essential recognition features. *Proc. Natl. Acad. Sci. USA.* 103:19326–19331.
67. Chen, B., M. U. Mayer, L. M. Markillie, D. L. Stenoien, and T. C. Squier. 2005. Dynamic motion of helix A in the amino-terminal domain of calmodulin is stabilized upon calcium activation. *Biochemistry.* 44:905–914.